Influence Of Impact Damage On Carbon-Epoxy Stiffener Crippling

Dawn Jegley

ABSTRACT

NASA, the Air Force Research Laboratory and The Boeing Company have worked to develop new low-cost, light-weight composite structures for aircraft. A Pultruded Rod Stitched Efficient Unitized Structure (PRSEUS) concept has been developed which offers advantages over traditional metallic structure. In this concept a stitched carbon-epoxy material system has been developed with the potential for reducing the weight and cost of transport aircraft structure by eliminating fasteners, thereby reducing part count and labor. By adding unidirectional carbon rods to the top of stiffeners, the panel becomes more structurally efficient. This combination produces a more damage tolerant design. This document describes the results of experimentation on PRSEUS specimens loaded in unidirectional compression subjected to impact damage and loaded in fatigue and to failure. A comparison with analytical predictions for pristine and damaged specimens is included.

INTRODUCTION

NASA, the Air Force Research Laboratory and The Boeing Company have worked to develop new low-cost, light-weight composite structures for aircraft. A Pultruded Rod Stitched Efficient Unitized Structure (PRSEUS) concept has been developed which offers advantages over traditional metallic structure [1]. In this concept a stitched carbon-epoxy material system has been developed with the potential for reducing the weight and cost of commercial transport aircraft structure. By stitching through the thickness of a dry carbon-epoxy material system, the labor associated with panel fabrication and assembly can be significantly reduced. When stitching through the thickness of pre-stacked skin, stringers, intercostals and spar caps, the need for mechanical fasteners is almost eliminated. This manufacturing approach reduces part count, and therefore, cost of the structure. In addition, stitching reduces delamination and improves damage tolerance, allowing for a lighter structure with more gradual failures than traditional composites without through-the-thickness reinforcement. However, the PRSEUS concept is relatively new and the behavior of PRSEUS specimens must be evaluated to understand how they respond to fatigue cycling and their failure response in the presence of low-speed impact damage.

Dawn C. Jegley, NASA Langley Research Center, mail stop 190 Hampton, Virginia 23681, U.S.A.

The PRSEUS concept consists of carbon-epoxy panels fabricated from dry

components and then infused in an oven while subjected to vacuum pressure. Skins, flanges and webs are composed of layers of graphite material forms that are prekitted in multi-ply stacks using Hercules, Inc. AS4 fibers. Several stacks of the prekitted material are used to build up the desired thickness and configuration. Specimens are stitched together using Vectran fibers. Stiffener flanges are stitched to the skin and no mechanical fasteners are used for joining. To maintain the panel geometry during fabrication, first stiffeners and then the skin are placed in a stitching tool for assembly prior to moving to a curing tool for consolidation in the oven. The stiffeners running in the axial direction consist of webs with a bulb of unidirectional carbon fiber rods at the top of the web. AS4 carbon fiber overwraps surround the bulb. The stiffeners in the lateral direction are foam filled hats. A sketch of the intersection of axial and lateral PRSEUS stiffeners is shown in figure 1 and a PRSEUS panel is shown in figure 2. Specimens in this study were cut from a similar panel.

Low-speed impact damage is often a critical design condition for composite structures in aircraft. The effect of impact-damage to a PRSEUS rod-stiffener is discussed herein. The objective of the present study is to compare the behavior of undamaged specimens loaded to failure in one cycle with specimens subjected to either impact, fatigue cycling, or both. Stiffener deformations such as crippling or buckling are of particular interest. Results are also compared to previous work with both PRSEUS specimens and with stitched blade-stiffened specimens [2-3].

TEST SPECIMEN DESCRIPTION

Four PRSEUS specimens were examined in the current study. All were cut from the same panel. This panel was composed of prekitted stacks of material, pultruded rods and Rohacell foam. The prekitted stacks had a $[45/\text{-}45/0_2/90/0_2/\text{-}45/45]_T$ laminate stacking sequence. Stack thickness was approximately 0.052 inches. The panel was made from AS4 fibers and HexFlow VRM 34 resin [1]. The pultruded rods were Toray unidirectional T800 fiber with a 3900-2B resin and the frame stiffeners were filled with Rohacell foam.

Each specimen contained a single rod-stiffener and no frame. The skin of each specimen was one stack of material with the 0 degree orientation aligned with the

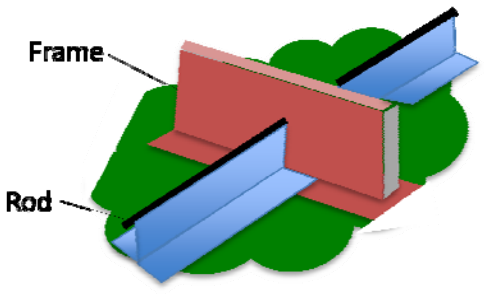

Figure 1. Intersection of PRSEUS stiffeners.

Figure 2. Typical PRSEUS panel.

stiffener. Nominal skin thickness was 0.052 but measured skin thickness ranged from 0.053 inches to 0.070 inches. A sketch of the cross section and a photograph of a typical specimen are shown in figures 3 and 4, respectively. Rod-stiffeners had a 3.4-inch wide flange, a 0.104 inch-thick stiffener web and a 1.5-inch tall stiffener. The nominal diameter of the pultruded rod was 0.375 inches and the nominal thickness of the overwrap was 0.052 inches. Measured diameter of the rod-overwrap region ranged from 0.478 inches to 0.494 inches. Flange thickness was half the web thickness. One stack of additional material was added under each flange and labeled as a tear strap in the figure. This reinforcing stack covered the same area of skin as the stiffener flange. Each specimen was 18 inches long and 6 inches wide. Prior to testing, each end of the specimen was potted in 1.0-inch-deep epoxy compound and the ends were ground flat and parallel to each other to ensure uniform load introduction.

A study of 12 blade-stiffened specimens is described in [3] and those results are repeated herein for comparison to PRSEUS results. In that study the specimens had the same fiber and stack as the PRSEUS specimens; however, Kevlar rather than Vectran threads were used and stitches were placed approximately every 0.25 inches in each direction rather than only two rows in the flange/skin region and two rows in the web. In addition, the specimens in [3] were fabricated in a resin film infusion autoclave process rather than in an out-of-autoclave process as with PRSEUS. None of these differences would be expected to have significant influence on the effect of impact. Blade specimens with the one- and two-stack skins were bonded back-to-back to create X-shaped specimens and suppress skin buckling to examine stiffener behavior. Specimens with a thicker flange and blade are T-shaped. Specimens were 12 to 14 inches long and 5 inches wide with a 3-inch tall blade. The cross sections of the blade specimens are shown in figure 5. Blade-stiffened specimens were potted in the same manner as the PRSEUS specimens. Photographs of an X-shaped and a T-shaped blade-stiffened specimen are shown in figure 6.

Three PRSEUS specimens were subjected to low-speed impact from a 25-lb drop weight impactor prior to testing. The impactor had a one-inch diameter tup. The impact arrangement is shown in figure 7. All specimens were impacted on the stiffener at the midlength location with the same weight/tup combination. Two specimens were impacted on the side of the rod with impact energy of 20 ft-lb and one was impacted on the top of the rod with a 20 ft-lb impact. 20 ft-lb represents the maximum damage likely to occur to the interior of the structure.

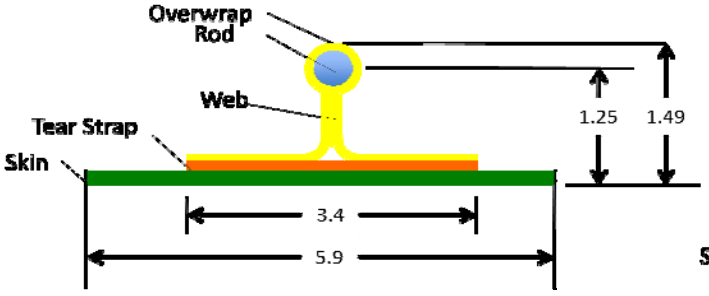

Figure 3. Specimen cross sectional geometry. Dimensions are in inches.

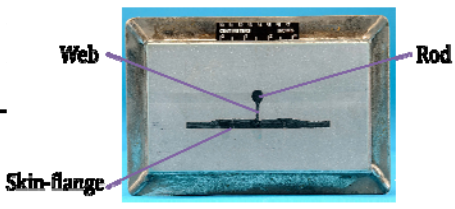

Figure 4. PRSEUS specimen cross section.

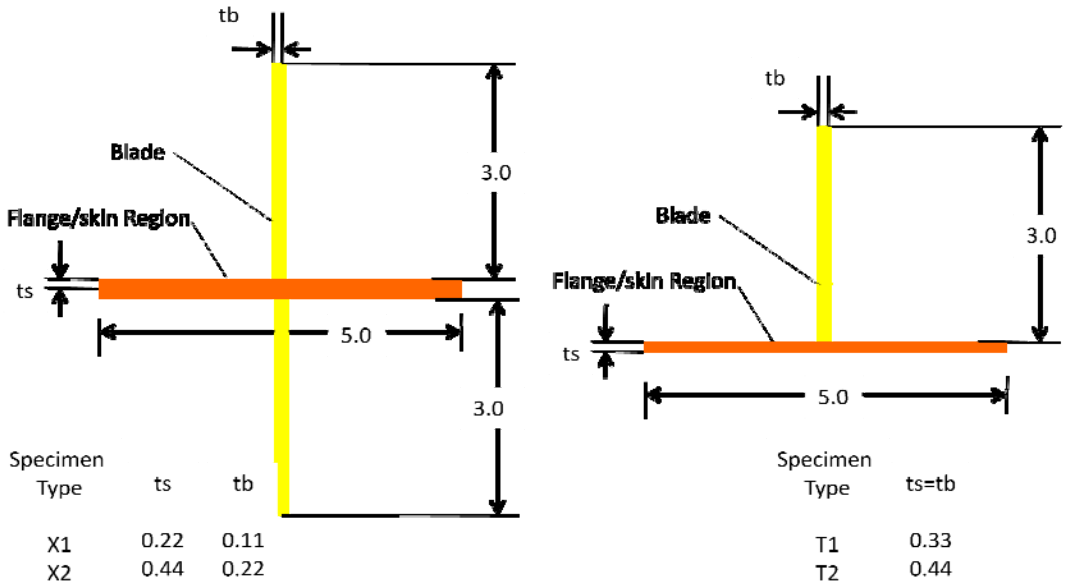

Figure 5. Cross-section of blade-stiffened specimens. Dimensions are in inches.

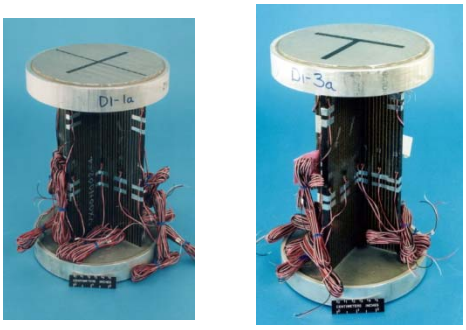

Figure 6. Blade stiffened specimen.

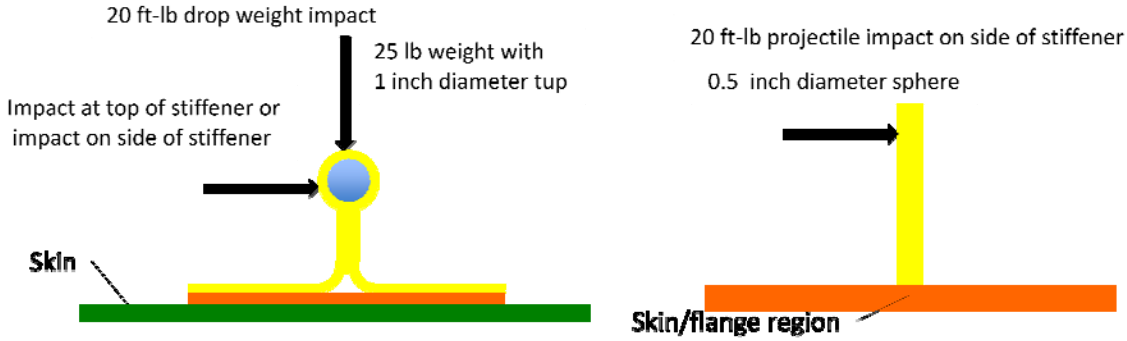

Figure 7. Impact locations.

Six blade-stiffened specimens were subjected to low-speed impact from an air-propelled aluminum spherical projectile with 0.5-inch diameter prior to testing. The impact arrangement is shown in figure 7. All specimens were impacted on the stiffener at the midlength location. These specimens were impacted normal to the blade with an energy level of approximately 20 ft-lb.

Impacts to PRSEUS stiffeners resulted in no visible damage for either the side or top impact, as shown in figure 8. Impacts to the blade-stiffened specimens resulted in obvious impacts as shown in figure 9. Even though the energy level is the same for the blade-stiffened specimens and the PRSEUS specimens, the smaller, lighter impactor inflicts damage over a smaller area and leaves more-visible evidence than the heavier impactor with the larger tup. This difference would have little effect for this situation.

TEST PROCEDURE AND INSTRUMENTATION

Some PRESUS specimens were loaded in fatigue and some were impacted prior to failure loadings. Some blade specimens were impacted but none were fatigued. All specimens were loaded to failure in axial compression. Of the four PRESUS specimens in the current study, one specimen was loaded to failure in a single static load test with no impact damage present to serve as a control specimen and for comparison to previous work. One specimen was impacted on the side of the rod-stiffener and then loaded to failure in a single loading cycle. Two specimens were subjected to fatigue loading of 55,000 cycles of compressive loading in the same manner as described in references 1 and 2. The 55,000 cycles was broken into 11 blocks of 5000 cycles with the maximum loads are shown in Table I for each cycle.

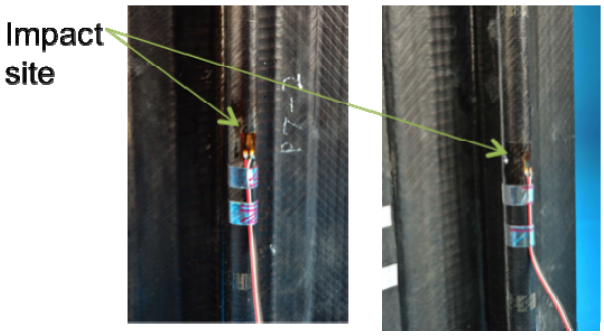

Figure 8. Impact damage site for PRSEUS specimens

Figure 9. Impact damage site for blade-stiffened specimens.

TABLE I. FATIGUE SPECTRUM FOR A SINGLE BLOCK*

	Load (lb)
Cycle 1	20,500 lb
Cycle 2-14	19,500 lb
Cycle 15-5000	18,500 lb

*5000-cycle blocks repeated 11 times for each specimen

A load rate of 1 Hz was used for all cycling except the first cycle of block 1, block 5 and the failure tests. Specimens were loaded in compression only and load was not removed between cycles but limited to a minimum of 200 lb. After the completion of the fatigue loading, each specimen was loaded to failure in axial compression. The first cycle of blocks 1 and 5 were recorded to determine if any change in specimen behavior occurred through the cycling. The load rate for these cycles was 0.01 in./min. Failure loading was also applied at the rate of approximately 0.01 in./min. The impacts and fatigue cycling details are shown in Table II.

Displacement and strain gage data were recorded at the rate of once every second as load was applied during the initial cycle and failure test. Displacements were measured using three displacement transducers measuring end-shortening, one measuring stiffener rolling and one measuring out-of-plane motion of the skin at the midlength location as shown in figure 10. Six strain gages were added to each specimen on the skin and rod in the pattern shown in figure 11. For the PRSEUS specimens, metal supports were added to the unloaded edges to restrain out-of-plane motion of the skin while allowing the specimen to deform in-plane. Since the skin of the blade-stiffened specimens was thicker, no edge supports were used. A specimen in the test machine is shown in figure 12. Buckling and failure behavior were noted for each specimen.

TABLE II. PRSEUS SPECIMEN IMPACTS AND CYCLES

Specimen identification	Impact energy (ft-lb)	Impact location	Loading cycles
1	none	N. A.	1
2	20	Rod top	55000
3	20	Rod side	55000
4	20	Rod Side	1

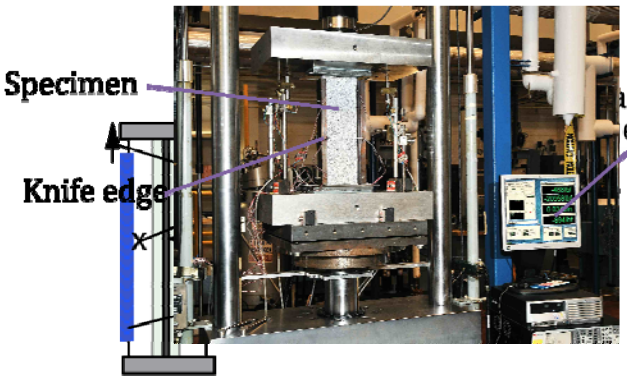

Figure 10. Displacement measurement locations.

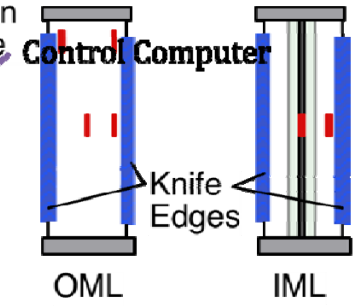

Figure 11. Strain gage locations.

Figure 12. Specimen in test machine.

An optical measurement system was used to obtain full-field displacement and strain results for the un-stiffened side of each specimen during the failure test. This Vision Image Correlation (VIC) system [4] requires a black and white speckle pattern to be painted on the specimen surface to allow the VIC system to track surface motion. Two cameras positioned at different angles to the specimen surface simultaneously photograph the specimen at set intervals during the test. In this case, the specimen was photographed every 0.5 seconds, resulting in approximately 1000 time steps of data for each test. The VIC system also records the load from the test machine so images can be related to the corresponding load. The VIC software compares the photographic images and produces three-dimensional displacements and strains at each time step. Since the full-field results are dependent upon the cameras having an unobstructed view of the surface, some local areas where strain gages or wires obstruct the view are removed from the full-field plots.

ANALYSIS APPROACH

Finite element analyses of the pristine PRSEUS specimen, a specimen in which a rod region was given reduced properties and a specimen with a severed rod (but intact web, flange and skin) were conducted to gage the influence of a loss of load carrying ability of the rod region. The analyses were conducted using the finite element code STAGS [5]. The analyses account for geometric nonlinearities but not plasticity. A buckling load was calculated based on a linear prebuckling stress state. Then a nonlinear analysis was conducted and buckling mode shapes were calculated based on the nonlinear stress state. Then an assumed initial imperfection in the shape of the buckling mode corresponding to the minimum buckling load was input. An imperfection mode with an amplitude of 0.002-inches was input to trigger nonlinear behavior.

Quadrilateral shell elements were used to model the skin, flange and web regions and beam elements were used to model the rod-overwrap region. The finite element model is shown in figure 13 and has 1320 nodes and 1275 elements, for a total of 8343 degrees of freedom.

All degrees of freedom on one end of the specimen were restrained. For a region of one inch from each end, i.e., inside the potted region, all degrees of

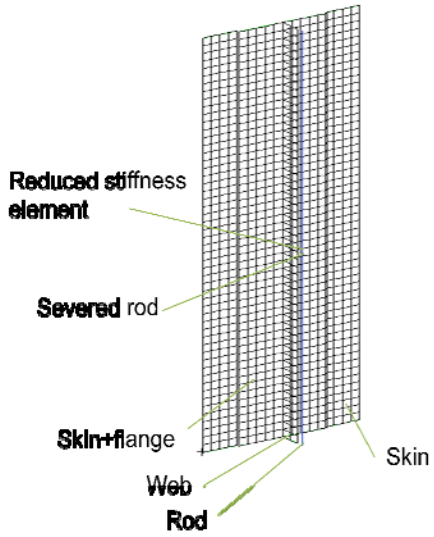
Reduced stiffness element
Severed rod
Skin+flange
Web
Rod
Skin

Figure 13. Finite element model of PRSEUS specimen.

freedom were restrained except for the shortening of the specimen. A load was applied on one end of the specimen and all nodes on that end were constrained to move the same amount. Knife edge supports were modeled by restraining out-of-plane motion along the unloaded edges at a row of nodes approximately 0.25 inches from the skin edge. The potting material was not modeled. Each configuration was analyzed to determine the linear, nonlinear and buckling behavior. Assumed properties are based on the compression properties for a stack of material [1], such that the axial stiffness is 9.23 Msi, the lateral stiffness is 4.66 Msi, the shear stiffness is 2.26 Msi, and poison's ratio is 0.397. The rod stiffness is assumed to be 18.5 Msi. In the reduced-stiffness model, the stiffness in the rod-overwrap region in one element at the midlength location was reduced by 50% but no other changes were made to the model. In the severed-rod model, the node between beam elements at the midlength location was duplicated but not connected, representing a discontinuity in the rod.

RESULTS AND DISCUSSION

Displacements, strains and failure modes are presented herein, followed by a comparison with data obtained previously for specimens with no impact damage. Full field results show displacement and strain distributions as the specimens approached failure.

Displacements and loads

Failure loads ranged from 38,091 to 45,080 lb for the four PRSEUS specimens examined in the current study, as shown in Table III. A comparison of their stiffness based on the applied load and end shortening is shown in figure 14. End-shortening measurements for the three loading platen locations indicate a uniform displacement was applied to the end of each specimen so the end-shortening shown was determined by averaging these three displacements. Data for

TABLE III. FAILURE LOADS OF PRSEUS SPECIMENS.

Specimen identification	Impact energy (ft-lb)	Impact location	Loading cycles	Failure load (lb)
1	none	N. A.	1	43,800
2	20	rod top	55000	39,028
3	20	rod side	55000	38,000
4	20	rod side	1	45,080
R1*	none	N. A.	1	48,500
R2*	none	N. A.	1	41,454
R3**	none	N. A.	55000	45,000
R4**	none	N. A.	55000	47,654

*Described in reference 1.
**Described in reference 2.

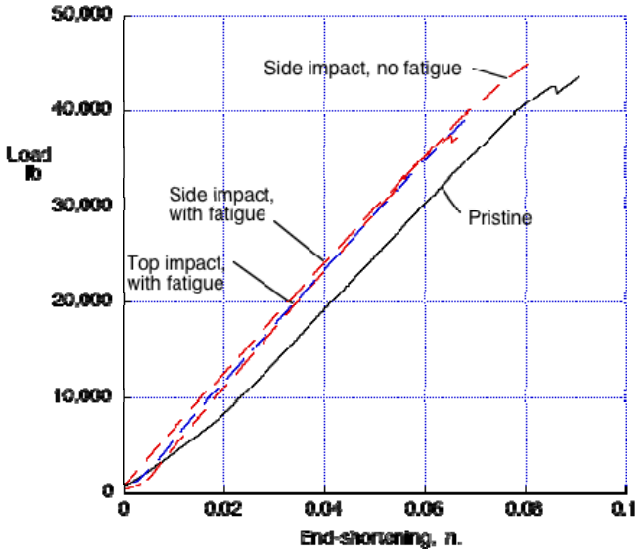

Figure 14. Load vs. end-shortening behavior.

the pristine specimen is shown as a solid black line and data for the impacted specimens are shown as dashed lines. Side impacts are shown in red and the top impact is shown in blue. The stiffnesses vary by approximately 10% however, the least stiff specimen is the pristine specimen with no cyclic loading so it is unlikely that this difference is related to the impact or fatigue but rather scatter in the specimens. From these limited results, there appears to be no effect of either fatigue cycles or impact to the rod-stiffener on the stiffness of the specimen.

Full-field results for out-of-plane deformation of the un-stiffened surface at approximately the maximum applied load are shown in figures 15-18 for specimens 1-4, respectively. In all the full-field results, regions where strain gages and wires obscure the specimen surface are removed from the plot. These out-of-plane results indicate all specimens buckled prior to failure. The centerline where the rod

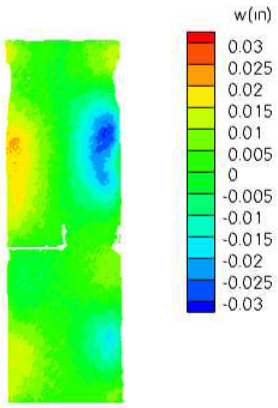
w(in)
0.03
0.025
0.02
0.015
0.01
0.005
0
-0.005
-0.01
-0.015
-0.02
-0.025
-0.03

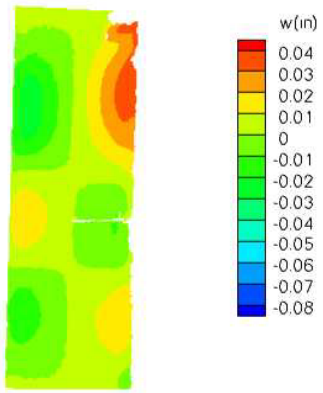

Figure 15. Full-field out of plane displacement at 43,785 lb for pristine specimen.

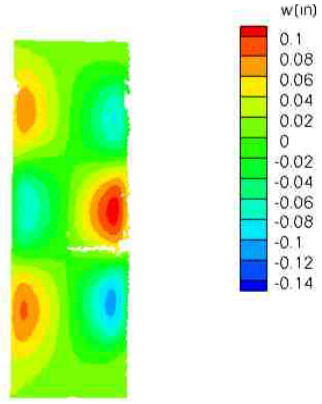

Figure 16. Full-field out of plane displacement at 39,064 lb for top impacted specimen after fatigue.

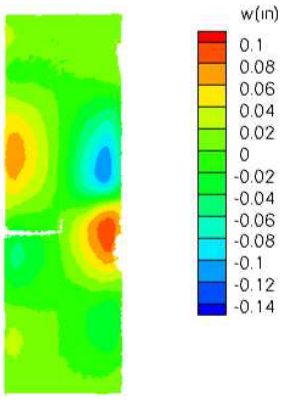

Figure 17. Full-field out of plane displacement at 38,102 lb for side impacted specimen after fatigue.

Figure 18. Full-field out of plane displacement at 45,286 lb for side impacted specimen with no fatigue.

was located did not move out-of-plane during loading while the unloaded edges did move out of plane despite the edge restraints. A buckle pattern of approximately three half waves developed in each specimen. In each specimen, at the centerline one edge moved in the positive z direction while the other edge moved in the negative z direction about the same magnitude. Impacts to the rod had no effect on the skin behavior.

The transducer on the stiffener indicates rolling of the web of the rod specimen at between 38,000 and 42,000 lb for the four specimens, which corresponds with the development of buckles in the skin.

The shortening of the control test specimen is shown with the corresponding analytical result in figure 19. The analytical result for the model with no assumed damage agrees well with the results for the control test specimen. The analytical prediction of the full-field out-of-plane displacement at a load of 38,000 lb is shown in figure 20 and shows the same pattern as found for the test as shown in figure 15.

.0123

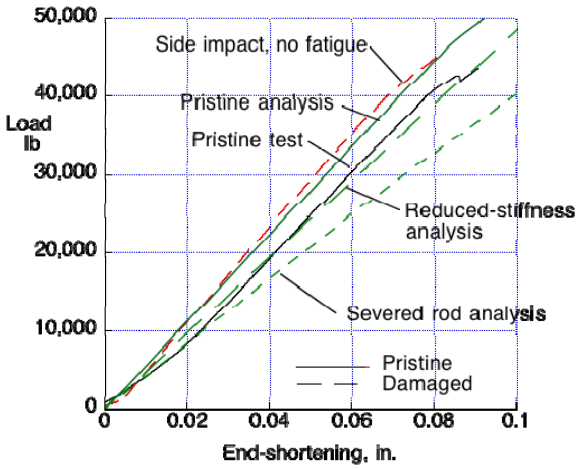

Figure 19. Load-shortening of pristine, reduced stiffness-rod and severed-rod analysis.

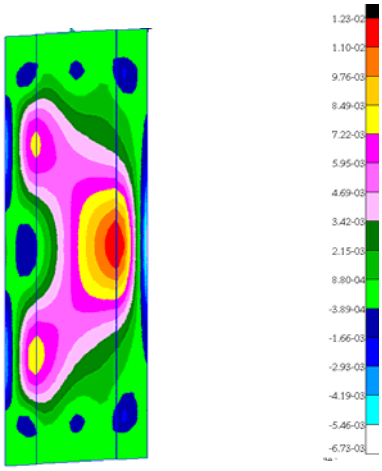

Figure 20. Analytically determined full-field out-of-plane deformation for pristine specimen at 38,111 lb.

The analytically determined shortening for the severed rod and reduced-stiffness rod are also shown in figure 19. Test data and the analytical prediction for the pristine specimen are shown as solid lines. Data for the impacted specimen with no fatigue is shown as a dashed red line and the analysis of the severed rod and the reduced-stiffness rod results are shown as dashed green lines. Little effect in this global measure of specimen behavior is seen due the locally reduced stiffness in the rod. Full-field-out-of-plane predictions for the reduced-stiffness rod and for the severed-rod analyses are shown in figures 21 and 22, respectively. Out-of-plane deformation is not significantly effected by the reduced stiffness but is effected by the severed rod.

Failure loads for all four specimens in the current study and four additional, nominally identical specimens are shown in Table III. Details of the additional specimens are presented in [1] and [2]. The specimens in these references were cut from a PRSEUS panel and prepared for testing in a similar manner but none of the

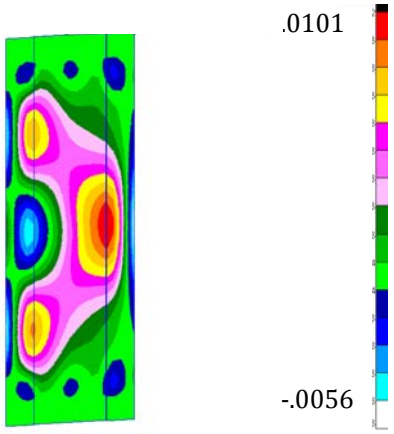

Figure 21. Displacement distribution in reduced-stiffness rod specimen at 38,000 lb.

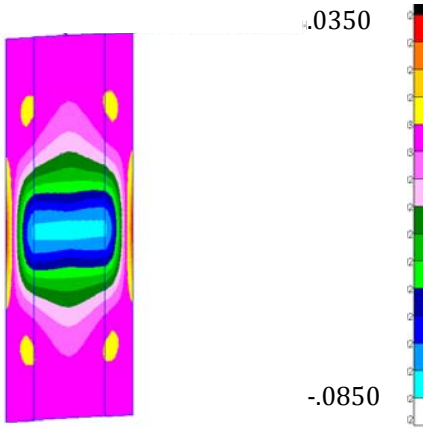

Figure 22. Displacement distribution in severed-rod specimen at 34,485 lb.

specimens in those references were impacted. Including all eight specimens, non-fatigued, non-impacted specimens failed at loads between 41,454 lb and 48,500 lb. Fatigued non-impacted specimens had failure loads within this range. The impacted but not fatigued specimen also had a failure load within this range. Fatigued, impacted specimens had failure loads slightly less than the lowest non-impacted failure, however, not enough specimens were examined to quantify the effect of impact. These results indicate that fatigue cycling alone had no impact on failure load and impact alone had no impact on failure load. However, impact followed by cycling may have reduced load-carrying ability by as much as 13%, as shown in figure 23.

The failure loads for the blade-stiffened specimens described in [3] are presented in Table IV. None of the blade-stiffened specimens were fatigued and all impacts were normal to the blade near the top edge. In general, the thicker the blade and flange, the more significant the effect of impact, but even with the four-stack blade and flange/skin, the reduction in load-carrying ability is only 15%, which is greater than the reduction of the non-fatigued PRSEUS specimen.

Strain

The load-strain relationship measured by the strain gage on the overwrap midlength for the pristine and impacted specimens are shown in figure 24. Data for the pristine specimen are shown as solid lines and data for the impacted specimen are shown as long dashed lines and data for fatigued specimens with no impacts are

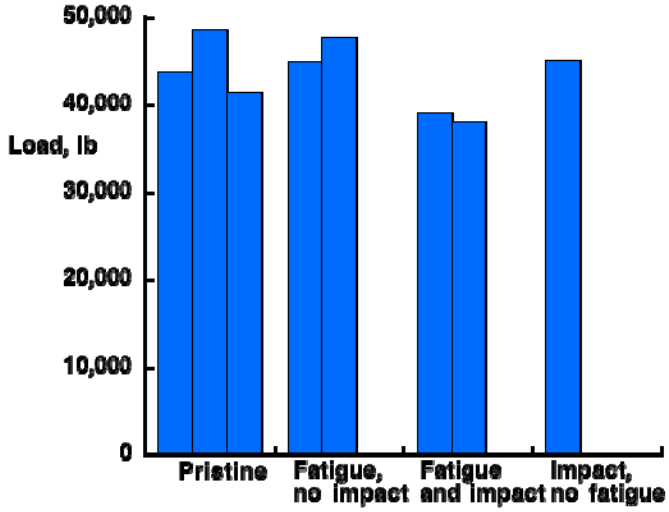

Figure 23. PRSEUS specimen failure loads.

TABLE IV. GEOMETRY AND FAILURE LOADS OF BLADE-STIFFENED SPECIMENS.

Specimen type	Web thickness (in.)	Flange/skin thickness (in.)	Length (in.)	Pristine (kips)	Impact-damaged (kips)	Percent reduction in load
X1	0.11	0.22	12	71	73	0
X2	0.22	0.44	13	192	176	8
T3	0.33	0.33	13	150 and 154*	137 and 141*	8
T4	0.44	0.44	14	231 and 254*	193 and 218*	15

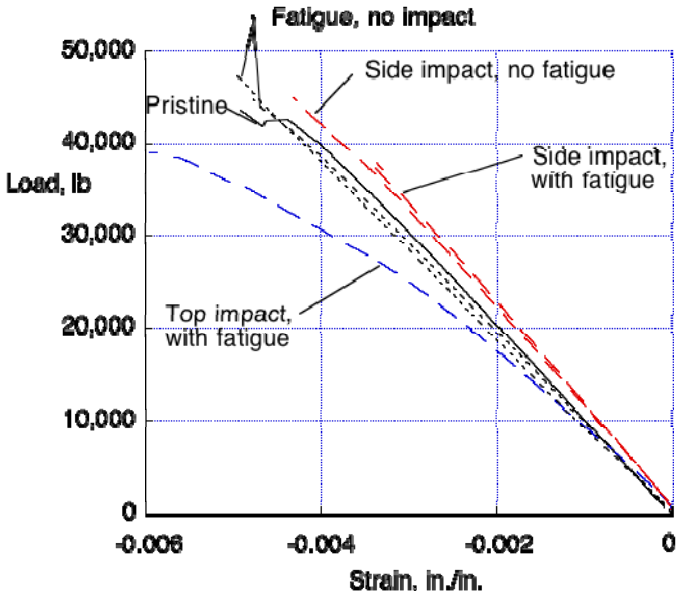

Figure 24. Strain on rod overwrap.

shown in short dash lines. The fatigue cycles had no effect on the behavior at this location for the unimpacted specimen. The impact at the top of the rod also did not significantly affect the behavior at this location, as shown by the dashed red lines. However, impact on the top of the rod may have caused enough damage to lead to nonlinear behavior of the gage at this location as shown by the long-dash blue line. It is important to note that while the impact affected the strain near the impact site, the fatigue cycles did not lead to a further change in the shape of the load-strain curve, as seen by comparing red lines representing side impact followed by fatigue and side impact without fatigue.

Full-field results for axial strains at approximately the maximum applied load are shown in figures 25-28 for specimens 1-4, respectively. The buckle pattern of three half waves in each direction is consistent with the strain distribution shown for the specimens. Peak strains are located above the axial centerline where the maximum strain magnitude for the control specimen is approximately 0.01 in./in. in

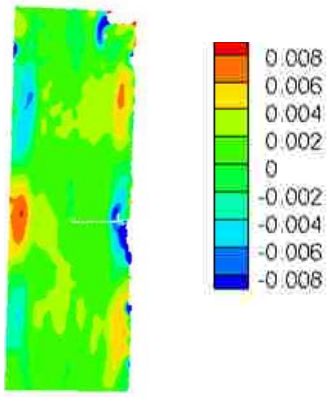

Figure 25. Full-field axial strain at 43,785 lb for pristine specimen.

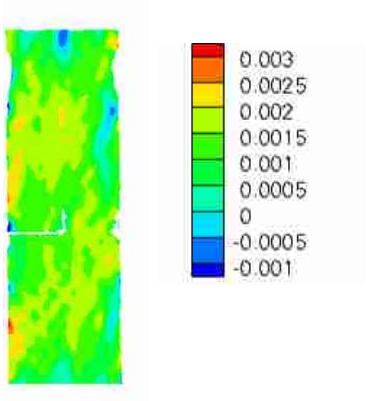

Figure 26. Full-field axial strain at 39,064 lb for top impacted specimen after fatigue.

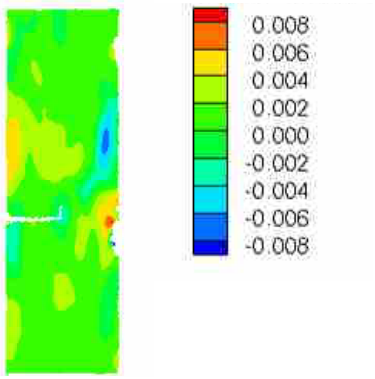

Figure 27. Full-field axial strain at 38,102 lb for side impacted specimen after fatigue.

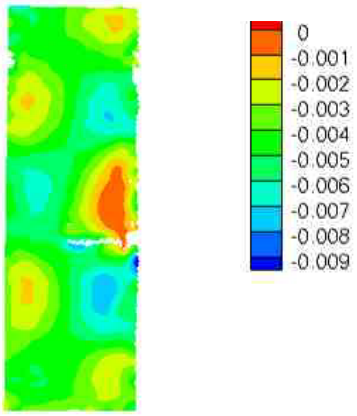

Figure 28. Full-field axial strain at 45,286 lb for side impacted specimen with no fatigue.

tension and approximately -0.01 in/in. in compression in the skin. Similar patterns are seen in two specimens impacted on the rod-stiffener. Impacts to the rod had no effect on the skin behavior.

Analytical strain results for the OML surface are shown in figures 29-31 for the pristine, reduced-stiffness rod, and severed-rod models, respectively. These results indicate that the strain in the region of the reduced stiffness is greater than the corresponding location in the pristine model but not significantly greater than the strain in the skin midlength, which is unaffected by the reduced stiffness rod region. Therefore, the analysis would indicate that the impact should have little effect on the compressive failure load. This conclusion is supported by the experimental results and implies that such non-visible damage may not require repair in a flight vehicle. The analysis with the severed-rod model shows significant increases in strain in the web where the rod is severed. This increase implies a significant

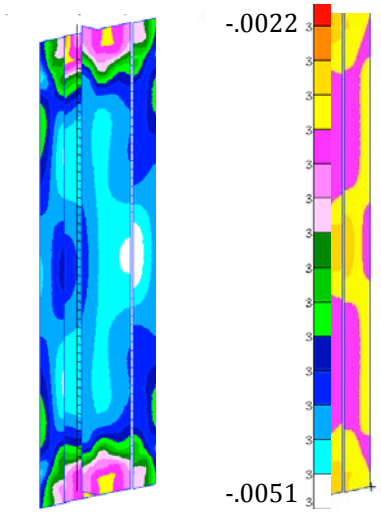

Figure 29. Analytically determined full-field axial strain at 44,000 lb for pristine specimen.

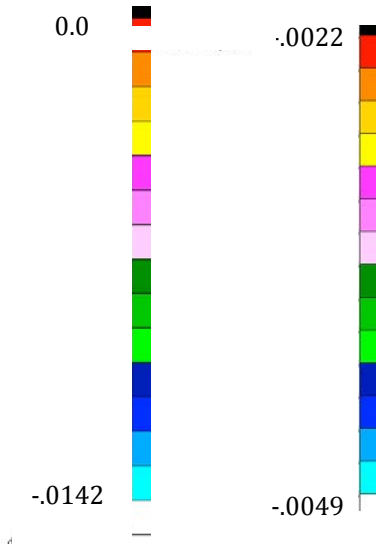

Figure 30. Analytically determined full-field axial strain at 44,000 lb for reduced-stiffness specimen.

Figure 31. Analytically determined full-field axial strain at 34,485 lb for severed-rod specimen.

reduction in failure load if the rod were damaged more severely, either fully severed or even partially severed. This result was not verified experimentally but indicates that such damage would require repair in a flight vehicle.

Failure

A comparison between failure loads obtained in the present study and those obtained in studies of nominally identical specimens with no impact damage are shown in figure 15 and Table III. Photographs of failed pristine and impacted specimens are shown in figure 32-35. These results indicate that fatigue cycling has no effect on failure loads and non-visible impact damage has only minimal influence on failure load or mode. In addition, fatigue cycling in the presence of impact damage did not influence the failure load any more than impact alone, implying there is no damage growth through the fatigue cycles.

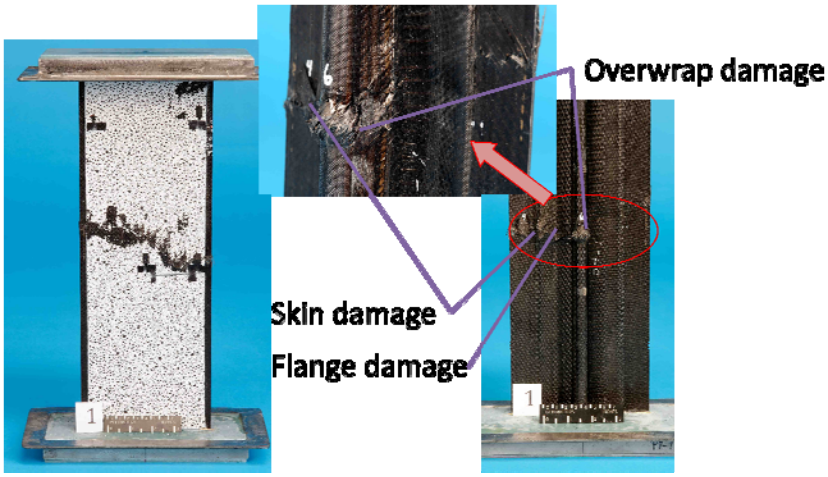

Figure 32. Failed specimen with no impact and no fatigue.

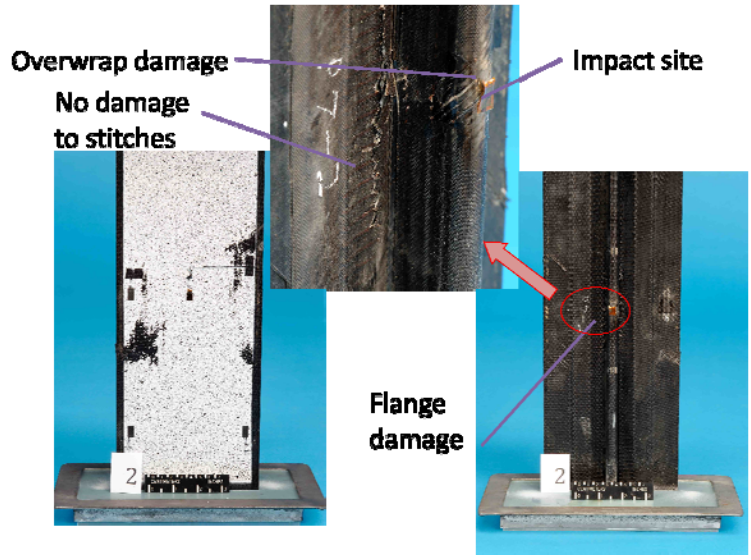

Figure 33. Failed specimen with top impact and fatigue.

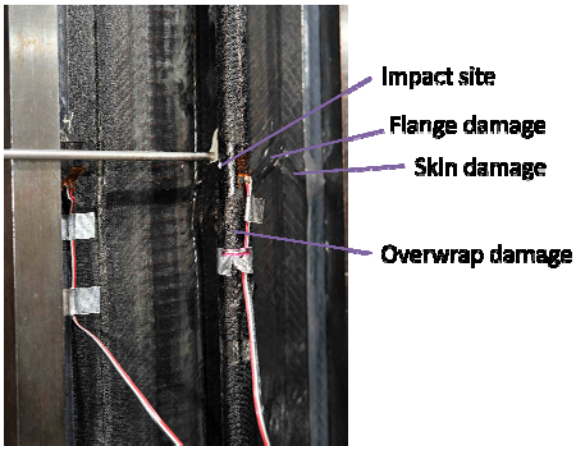

Figure 34. Failed specimen with side impact and fatigue.

Figure 35. Failed specimen with side impact and no fatigue.

Rod-stiffened specimens failed midlength across the full width of the specimen. Minimal delamination can be seen between the flange and skin. Overwrap damage can be seen around the rod. Specimens R3 and R4 failed in the same manner [2].

APPLICATION TO HYBRID WING BODY VEHICLE

A currently proposed application for the PRSEUS concept is a hybrid wing body vehicle. This study addresses the streamwise loading (Nx) in the center region of the upper and lower cover panels in the center section when Nx is in compression. The critical loadings for the upper and lower cover panels in the version of the vehicle described in reference 1 are the 2.5G upbending condition for the upper cover and the -1G downbending condition for the lower cover.

The running loads from the global finite element model presented in [1] provide a basis for comparison for the results of the current study. PRSEUS would be applied such that the rod-stiffeners would run from nose to tail in the center section. The regions of the cover panels where design ultimate running load is less than the failure running load for the impacted, fatigued specimens described herein are shown in green in figures 36 and 37 for the upper cover and lower cover, respectively. The current configuration would not be adequate for the red regions. Note that the center section is green in both figures. This configuration is only applicable to the center section of the aircraft since additional build-ups at the side of body region would be required and the direction of the rod-stiffeners would be different in the wing regions than in the center section.

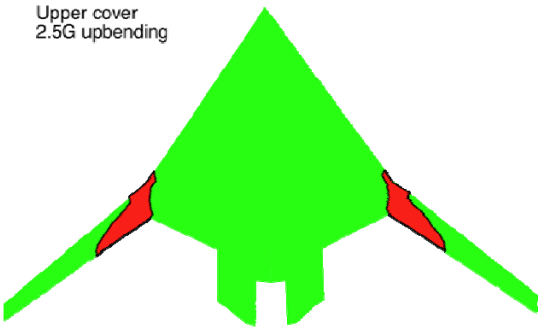

Figure 36. Upper cover of hybrid wing body aircraft.

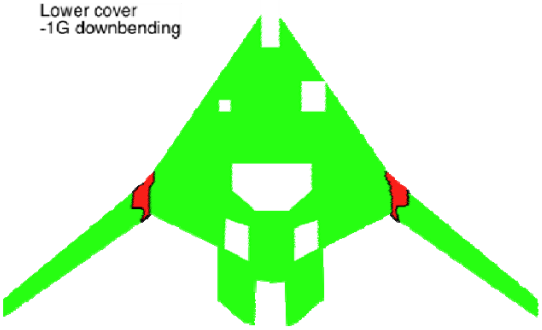

Figure 37. Lower cover of hybrid wing body aircraft.

CONCLUDING REMARKS

Single-stiffener specimens fabricated using a Pultruded Rod Stitched Efficient Unitized Structure (PRSEUS) concept in an out-of-autoclave process were evaluated. Experimental results from nominally identical compression-loaded specimens subjected to one or 55,000 cycles of loading with and without impact damage were obtained. These results indicate that fatigue cycling an initially pristine specimen has no effect on failure loads and non-visible impact damage resulting from an impact of energy 20 ft-lb to the stiffener has no effect on load-carrying ability for single loadings to failure so this level of damage would not need to be repaired. However, the combination of impact to the stiffener and 55,000 cycles of compressive loading may reduce the failure load by as much as 13 percent. Analysis indicates that more severe damage would need to be repaired because of stress concentrations that could lead to failure just outside the damage region. Because of the limited number of specimens in the current study, the trends seen warrant additional investigation but are an initial indication of the impact and fatigue behavior of PRSEUS specimens. This limited study also indicates that PRSEUS specimens perform at least as well as the stitched blade-stiffened specimens previously studied.

REFERENCES

1. Velicki, A. 2009. "Damage Arresting Composites for Shaped Vehicles," NASA CR-2009-215932.
2. Jegley, D. 2009. "Experimental Behavior of Fatigued Single Stiffener PRSEUS Specimens," NASA TM-2009-215955.
3. Jegley, Dawn C. 2005. "Structural Efficiency Of Stitched Composite Panels With Stiffener Crippling." Journal of Aircraft, Vol. 42, No. 5, pp. 1273-1280, September-October, 2005.
4. McGowan, David M., Ambur, Damodar R., and McNeil, Stephen R. 2003. "Full-field Structural Response of Composite Structures: Analysis and Experiment," presented at the 44th AIAA/ASME/ASCE/AHS Structures, Dynamics and Materials Conference, AIAA 2003-1623, Norfolk, VA, April 2003.
5. Rankin, C. C., Brogan, F. A, Loden, W. A., and Cabiness, H. D. 2001. "STAGS User Manual, Version 4.0." Lockheed Martin Missiles and Space Company, Incorporated.